# Optimization of Laser Directed Energy Deposition (LDED) Additive Manufacturing Process with High-Speed IR cameras

by

Siddharth Khanna

Supervisor: Professor Yu Zou
Date: April 7th, 2025

**B.A.Sc. Thesis**

Division of Engineering Science
UNIVERSITY OF TORONTO

# Abstract

This thesis investigates the optimization of the Laser Directed Energy Deposition (LDED) process by leveraging high-speed infrared (IR) thermal imaging and data-driven analysis to improve print quality assessment. While LDED offers significant advantages for additive manufacturing of complex and high-value metal components, it remains prone to variability due to the dynamic and nonlinear nature of the melt pool.

To address this, a high-throughput experimental framework was developed, enabling systematic exploration of over 360 unique process parameter combinations involving laser power, scan speed, and feed rate. In situ thermal data captured via a high-speed IR camera was used to extract key dynamic features—including melt pool stability, morphology, and sputter density—while post-process measurements provided static geometric features such as track height and surface roughness.

Among the dynamic indicators, melt pool stability—quantified through steady-state duration and coefficient of variation—emerged as the most reliable predictor of print quality. In contrast, features like morphology and sputter density showed no consistent correlation with outcomes. A suite of machine learning models, including decision trees, ensemble methods, and neural networks, was then trained to predict quality metrics using both static and dynamic features.

The best performance was achieved when combining melt pool stability with surface roughness, with neural networks and ensemble models yielding high $R^2$ scores ($> 0.84$), demonstrating the power of hybrid feature sets. These findings emphasize the value of integrating real-time monitoring with post-process evaluation and lay the groundwork for closed-loop control in LDED manufacturing workflows.

# Acknowledgements

I would like to thank my supervisor, Professor Yu Zou, for his invaluable guidance and expertise throughout this thesis. His insight into LDED technology and his continuous support fostered both technical understanding and personal growth. I am also especially grateful to JiaHui Zhang for providing experimental assistance, thoughtful advice, and direction during critical stages of the project. Their combined support has deeply enriched the content of this work and strengthened my passion for research.

# Contents

# List of Figures

# List of Tables

# 1 Introduction

Laser Directed Energy Deposition (LDED) has emerged as a promising technique in metal additive manufacturing due to its ability to fabricate complex geometries and repair high-value components with minimal material waste [1, 2, 3]. In the LDED process, a high-power laser beam melts metallic powder as it is fed onto a substrate, forming a molten pool that rapidly solidifies to create metallurgical bonds. The coordinated interaction between the laser beam and powder delivery system enables the production of customized, high-integrity parts, especially thin-walled structures required in aerospace and biomedical sectors [4].

Thin-walled geometries are particularly sensitive to processing variations due to their limited dimensional tolerance. The formation of each layer is governed by the stability and geometry of the single-track melt pool, making it crucial to optimize process parameters such as laser power (P), scan speed (v), and powder feed rate (f) at the individual track level [5, 6, 7]. Poor control over these parameters may result in defects like porosity, lack of fusion, or inconsistent surface roughness [8, 9].

Traditionally, print quality has been assessed using static geometric metrics such as melt pool height, width, and surface roughness [10, 11]. However, these post-process measures fail to capture the highly transient and stochastic nature of melt pool behavior. Thermal instabilities—including fluctuations in melt pool size, Marangoni convection, and spattering—can develop over microsecond timescales, with significant implications for print quality in multi-layer builds [12, 13, 14].

To better understand and control these instabilities, recent studies have explored the use of real-time, in-situ monitoring systems. High-speed infrared (IR) imaging has proven especially effective in capturing rapid thermal and spatial changes in the melt pool with high temporal resolution [15, 16, 17]. These imaging techniques enable dynamic observation of melt pool evolution and provide an opportunity to detect and mitigate anomalies as they occur.

Coupled with this advancement is the use of high-throughput experimental frameworks capable of sampling a wide range of process parameter combinations. By integrating thermal imaging with automated data collection systems, researchers can now generate structured datasets suitable for machine learning (ML) and statistical analysis [18, 19, 20]. Dynamic features such as melt pool area fluctuation, relative stability, and sputter density have emerged as valuable indicators for assessing deposition quality in real-time [21].

At the same time, post-process geometric features like track height, cross-sectional area, and surface roughness continue to provide insight into material consolidation and deposition efficiency. By combining both dynamic and static features, a more holistic picture of process

behavior and its influence on part quality can be achieved.

This thesis aims to develop an in-situ monitoring and machine learning framework that integrates both real-time thermal data and post-process geometric features to predict print quality in LDED. A high-speed IR camera will be employed to monitor melt pool evolution across a large design space of process parameters. Through feature extraction and regression modeling, this study seeks to identify optimal parameter sets for stable, high-quality deposition. The overarching objective is to move towards a more intelligent and adaptive LDED process by bridging real-time sensing with predictive analytics.

# 2 Background And Related Work

## 2.1 LDED Process Overview

Laser Directed Energy Deposition (LDED) is a Directed Energy Deposition (DED) technique that has gained increasing attention in recent years for its ability to fabricate large, near-net shape components and repair high-value parts. Unlike Powder Bed Fusion (PBF) processes, LDED relies on a laser beam that melts metal powder delivered through a coaxial nozzle directly onto a substrate. This enables flexible toolpath programming, faster build rates, and compatibility with a wide range of materials [22].

Compared to other AM methods, LDED offers advantages in terms of part size, material efficiency, and application versatility. However, its open-loop nature, reliance on manual parameter tuning, and sensitivity to disturbances make it prone to various defects including porosity, delamination, cracking, and poor surface finish [23, 24]. To tackle these challenges, the development of real-time monitoring and adaptive control strategies has become essential.

## 2.2 Defects and Process Instability in LDED

Defects in LDED are often caused by inconsistencies in the melt pool due to unbalanced thermal conditions, which can be triggered by improper parameter selection or environmental fluctuations [8]. For instance, excessive energy input can lead to keyholing or spattering, while insufficient power may result in lack of fusion. The morphology of the melt track and melt pool stability are critical to ensuring consistent layer deposition and mechanical integrity.

Thermal instability also impacts geometrical features such as melt pool depth and width, which directly influence dilution, bonding quality, and structural accuracy. Studies have demonstrated that melt pool characteristics like area, aspect ratio, and fluctuation rates are

key indicators of deposition quality [9].

### 2.3 Machine Learning in LDED Monitoring

Recently, machine learning (ML) has emerged as a powerful tool to understand the complex, non-linear relationships between processing parameters and print quality. By leveraging high-resolution thermal data, ML models have shown the potential to predict features such as porosity, melt pool dimensions, and even surface quality [25, 26].

For example, Mi et al. used thermal features to predict porosity using decision trees and neural networks, achieving notable accuracy on unseen data [25]. Similarly, Tang et al. trained convolutional neural networks (CNNs) on melt pool thermal images to classify defect types and quantify porosity in real time [26]. These approaches highlight the growing relevance of data-driven models in augmenting traditional empirical and physics-based understanding.

### 2.4 Need for Feature Fusion and Stability Metrics

While traditional quality metrics such as melt track height and dilution provide insight into final part geometry, they often fail to capture transient process dynamics. Incorporating dynamic features—such as melt pool area fluctuations, stability duration, and surface roughness variation—has been shown to improve the robustness of predictive models [23].

Stability metrics, which quantify the consistency of melt pool behavior over time, are increasingly being used as a proxy for deposition quality. These include the coefficient of variation and steady-state duration, both of which help identify unstable process conditions that might otherwise go undetected through static measurements alone.

## 3 Materials and Methodology

### 3.1 In Situ Thermal Monitoring of the LDED Process

A custom-built Laser Directed Energy Deposition (LDED) platform was used to fabricate all samples in this study. The system included a three-axis motion platform and a continuous-wave fiber laser (IGA Photonics, $\lambda = 1070$ nm) capable of delivering up to 1 kW of nominal power. The laser beam was focused to a fixed spot radius of 500 $\mu$m across all experiments. The powder was delivered using a coaxial printing nozzle (COAX14 v5, Fraunhofer USA, Inc.), which directed the metal particles evenly into laser path while simultaneously supplying

argon gas to act as both the carrier and shielding medium to reduce oxidation during the process.

The metal powder used was gas-atomized 316L stainless steel, with a particle size distribution of 15–45 $\mu$m. A PLC-controlled powder feeder (PF 2/2, GTV GmBH), linked to a mass flow meter, ensured consistent and accurate powder delivery across all trials. The substrate on which the metal powder was deposited was a 316L stainless steel plate with a thickness of 12.7 mm. All substrates were prepared with 60-grit sandpaper prior to printing to improve adhesion and maintain consistent surface conditions

To capture the melt pool behavior in real time, a high-speed infrared (IR) camera (Telops M1K) was mounted at an off-axis angle of approximately 80 degrees from the laser path. This provided a wide and unobstructed view of the substrate and the melt pool during printing. The camera recorded thermal data at 2000 frames per second with a resolution of 320×160 pixels and an exposure time of 15 $\mu$s. The temperatures captured by the camera were calibrated between 250°C and 2062°C, with melt pool boundaries identified using a thermal threshold near the melting point of 316L stainless steel ($\sim$1400°C). For temperature mapping, an emissivity value of 0.3 was used based on prior literature [19].

To prevent heat buildup between successive melt tracks, the substrate was mountaed on a water cooled copper heat sink, secured with thermaly conductive past. This ensured the substrate temperature was consistenly below 100°C throughout the experiments, as confirmed by continuous thermal imaging. All video recordings and thermal data were saved for offline analysis, which included calculating the melt pool area and extracting print stability metrics.

This integrated system allowed for precise tuning of the LDED process parameters and detailed, high-resolution observation of melt pool dynamics.This provided a solid foundation for evaluating deposition stability and developing machine learning models to predict print quality.

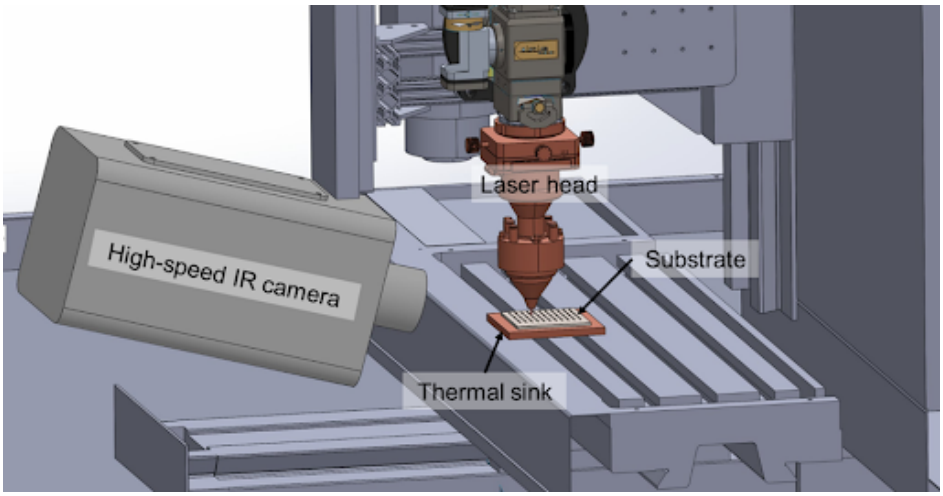


Figure 1: Schematic of the in situ monitoring setup showing the integration of a high-speed infrared (IR) camera with a customized Laser Directed Energy Deposition (LDED) system. The camera captures real-time thermal data from the melt pool during deposition onto the substrate, which is mounted on a thermal sink for heat dissipation.

## 3.2 High-Throughput Experiments for Melt Track Fabrication and Characterization

A wide range of process parameters was tested to evaluate how different printing conditions affect the melt pool behavior and track geometry. In total, 360 unique parameter combinations were tested by systematically adjusting the laser power ($P$), scan speed ($v$), and powder feed rate ($f$). Specifically, $P$ ranged from 310 W to 600 W in increments of 10 W, $v$ was adjusted from 4 mm/s to 12 mm/s in 4 mm/s steps, and $f$ was tuned from 0.2 rpm to 0.8 rpm in steps of 0.2 rpm. Each combination was printed twice to ensure repeatability and consistency.

All tracks were deposited as 100 mm-long, single-layer lines. The experiments were distributed over four identical 316L stainless steel substrates, each assigned to one of the four different feed rates. The tracks were spaced 4 mm apart in both horizontal and vertical directions to avoid thermal overlap and ensure clear visibility for the camera.

Once the tracks were printed and data collected using the high-speed IR camera, the samples were sectioned and prepared for metallographic examination to evaluate internal melt pool geometries. This preparation included mechanical grinding using 600-, 800-, and 1200-grit sandpapers, followed by polishing with a 0.1 $\mu$m suspension. Etching was performed using 50% concentrated Carpenter's reagent to reveal melt pool boundaries. A webcam (Omron Sentech Co., Ltd.), mounted directly onto the deposition system, was used to automate image capture of the cross-sections.

To extract surface-level geometric features, a subset of melt tracks was also scanned using a fully automated digital microscope (Keyence VHX-7000). These 3D surface scans provided accurate quantitative data on static features including track height, width, surface roughness, and deposited volume. These measurements were later used as morphological inputs for machine learning analysis.

This high-throughput workflow enabled the rapid generation of a comprehensive dataset linking process parameters, in situ thermal behavior, and resulting geometric outcomes. These data streams were subsequently integrated into a machine learning pipeline, described in later sections, for model development and analysis.

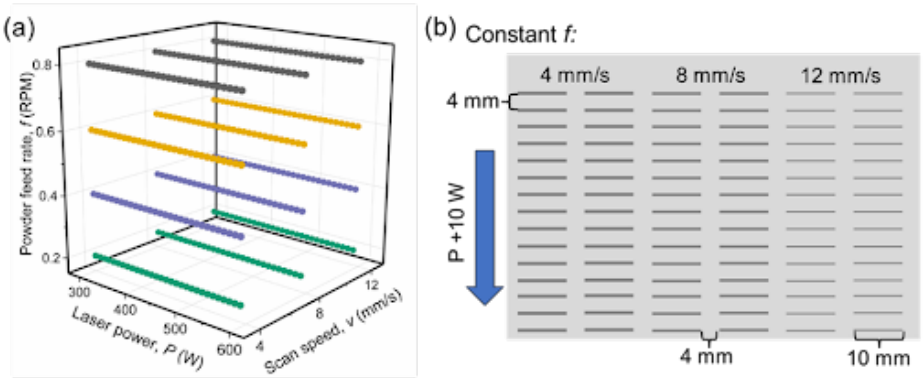


Figure 2: Schematic diagram of the high-throughput experiments: (a) Selected processing parameters in the laser power–scan speed–feed rate space, and (b) Experimental design for fabricating single-layer melt tracks at constant feed rate with varying laser power and scan speed.

## 3.3 Printing Stability Evaluation

To understand how the melt pool behaves over time and to quantify its stability under the different processing conditions, the thermal video data captured using the high-speed IR camera were post-processed using a custom computational pipeline. Due to the camera's high spatial and temporal resolution, each melt track generated thousands of thermal images, offering a detailed view of melt pool evolution throughout the entire printing process. This allowed for clear identification of consistent deposition phases and revealed how different combinations of process parameters influenced melt pool dynamics.

Each melt track video contained between 2000 to 6000 frames, depending on the scan speed. To evaluate each frame, an automated MATLAB script was used. The first step involved detecting the melt pool boundaries based on pixel intensity values corresponding to thermal emissions. The temperature threshold selected was approximately 1400°C (the melting point of 316L stainless steel). This isolated the active melt pool from cooler re-

gions, spatter, and reflections on the substrate, ensuring that only the melt pool region was calculated and analyzed.

Once the frames were processed, the melt pool area was plotted for each of the 360 experiments. To reduce high-frequency noise in the raw signal, a moving average filter with a window size of 80 frames was applied. This value worked reliably across all prints, helping to identify fluctuations and transitions more clearly. The first derivative of the smoothed area signal was then computed to detect trend changes, which were used to define the start and end of the stable region. The start point was typically identified by setting the derivative threshold near zero, capturing the local maximum that marked the end of the initial ramp-up phase. The end point was identified by setting the derivative threshold around $-1$, corresponding to the sudden drop in melt pool area. These thresholds were slightly adjusted in some cases to account for noise and sharp transitions, allowing consistent isolation of the stable region across all parameter combinations.

Printing stability is controlled by the thermal balance between laser energy input and heat dissipation into the surrounding material. Disruptions to this balance can cause melt pool fluctuations, which may lead to defects and irregular track formation. To capture this behavior quantitatively, two metrics were calculated for each melt track:

- **Stability Duration (%)**: Defined as the percentage of frames between the identified start and end points, indicating the actual *stable* region, excluding the initial ramp-up and power-down phases. This metric captured the portion of the print where stable energy absorption and consistent material interaction occurred.
- **Coefficient of Variation (CV)**: Calculated as the ratio of the standard deviation to the mean of melt pool area during the stable region. A lower CV indicates more uniform melt pool behavior, which correlates with better track consistency and fewer defects.

These indicators served as quantitative proxies for print quality and were extracted for all 360 process conditions. By tracking melt pool area fluctuations at high resolution, this method provided a dynamic understanding of process behavior, highlighting regions of both stable and unstable deposition. The results from this analysis were later used as inputs for data-driven modeling and process optimization strategies described in subsequent sections.

## 3.4 Melt Pool Morphology

The melt morphology analysis was carried out to evaluate the geometric consistency of the melt pool during deposition. The goal was to measure how closely the observed melt

pool shape matached an ideal reference geometry, which would represent a stable and well-controlled printing condition..

Because the camera was mounted at an approximately 80-degree viewing angle, there was some perspective distortion in the captured images The true melt pool shape on the substrate is generally circular however, due to the distortion, the melt pool appears elliptical. To correct for this, a known circular reference object was used to calibrate the distortion and calculate the scaling factor.

Using this calibration, a MATLAB script was developed to automatically generate an elliptical mask for each frame based on the melt pool width. The mask represented the expected melt pool shape as viewed from the camera. It was then overlaid onto the segmented melt pool region, and the degree of overlap was computed for each frame. These values were then averaged and used to quantify how well the actual melt pool conformed to the predicted shape throughout the print.

This method enabled consistent, frame-by-frame evaluation of melt pool morphology across all parameter sets, providing a dynamic shape-based feature that could potentially reflect process quality or deviation.

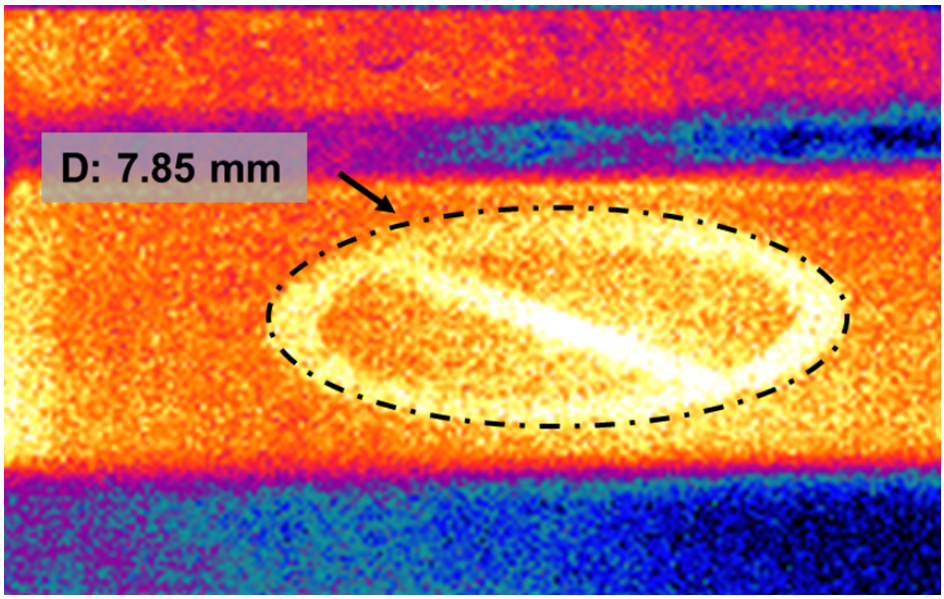


Figure 3: Infrared thermal image of a circular stop sign with known diameter (D = 7.85 mm) used to quantify geometric distortion in the imaging system. The elliptical appearance indicates spatial distortion, which is measured to correct for lens or perspective-related errors.

## 3.5 Sputter Density Extraction

During the printing process, high-temperature sputter was visible near the melt pool and this was analyzed as another dynamic feature using the same thermal imaging data. Unlike melt pool segmentation, which retains only pixels above the melting threshold, the sputter analysis focused on identifying pixels outside the melt pool region.

To achieve this, a lower threshold of approximately 500°C was applied to remove background noise while still retaining low-temperature sputters. Next, the melt pool location and size were used to define a bounding box, which was then used to remove the melt pool region from each frame.

Pixels that remained after this exclusion were classified as sputter particles. The number of these pixels was counted frame by frame and summed over the full duration of the print to generate a single sputter density value for each melt track

This method enabled consistent quantification of sputter activity under varying process conditions, providing an additional dynamic descriptor of thermal and material behavior during deposition.

## 3.6 Static Geometric Features

In addition to the dynamic features, a set of static geometric features were extracted from the melt track after printing to provide a more in-depth evaluation of print quality. These features included melt track height, melt track width, cross-sectional area, and surface roughness.

To obtain this data, a subset of melt tracks was scanned using a fully automated digital microscope (Keyence VHX-7000), which provided high-resolution 3D surface profiles of the deposited material. Each scan was aligned along the center of the track, and measurements were taken at consistent locations across all samples to ensure comparability.

Track height was defined as the vertical distance from the substrate surface to the peak of the melt track, while track width referred to the horizontal extent of the deposited material at the base. The cross-sectional area was estimated by integrating the surface profile across the width of the track. This method assumes symmetric deposition. Finally, surface roughness was evaluated using the built-in tool of the Keyence system, which calculates the $R_a$ values based on the scanned geometries.

## 3.7 Machine Learning Pipeline

To evaluate how well different combinations of process parameters could predict specific indicators of print quality, a set of machine learning models was developed using both dynamic and static features. These models also assessed whether including post-process geometric data, such as surface roughness, would improve prediction accuracy.

Four separate models were created, each focused on a different output feature related to the LDED process:

1. Melt Track Height
2. Melt Pool Area
3. Melt Pool Stability
4. Melt Pool Stability + Surface Roughness

Each model was made to understand how well the process parameters could predict a specific print-related feature, and whether the inclusion of additional static geometry (like surface roughness) added value.

The following regression algorithms were selected based on their ability to capture both linear and non-linear relationships between variables:

- **Linear Regression (LR)**: Used as a baseline due to its simplicity and computational efficiency.
- **Decision Tree (DT)**: Implemented to capture non-linear relationships between features.
- **Extra Trees (ET)**: An ensemble tree-based method used to improve generalization and reduce overfitting. Hyperparameters such as the minimum leaf size and number of learners were tuned.
- **Neural Networks (NN)**: Applied for their capacity to learn complex non-linear patterns; hyperparameters included the number of hidden layers and neurons per layer.

All models were trained and validated using a five-fold nested cross-validation, with an 80:20 train–test split. Hyperparameter optimization was performed using Bayesian optimization with an improvement-based acquisition function.

Model performance was evaluated using the following three metrics:

- **Root Mean Square Error (RMSE)**: Measures the average magnitude of prediction error.

$$\text{RMSE} = \sqrt{\frac{1}{T}\sum_{t=1}^{T}(\hat{y}_t - y_t)^2} \tag{1}$$

- **Mean Absolute Percentage Error (MAPE)**: Expresses the prediction error as a percentage of the actual value.

$$\text{MAPE} = \frac{100}{T}\sum_{t=1}^{T}\left|\frac{\hat{y}_t - y_t}{y_t}\right| \tag{2}$$

- **$R^2$ Score (Coefficient of Determination)**: Indicates the proportion of variance in the output that is explained by the model. This metric was only calculated for the melt pool stability and melt pool stability + surface roughness models.

$$R^2 = 1 - \frac{\sum_{t=1}^{T}(\hat{y}_t - y_t)^2}{\sum_{t=1}^{T}(y_t - \bar{y})^2} \tag{3}$$

Here, $\hat{y}_t$ and $y_t$ denote the predicted and actual print quality scores for the $t$-th sample, respectively, and $\bar{y}$ is the mean of the actual scores.

By comparing models trained with and without static features, this approach enabled a direct assessment of the added value of post-process geometric information beyond real-time dynamic monitoring. It provided insights into which features were most predictive of print quality across the 360-track dataset.

# 4 Results

## 4.1 Melt Pool Dimension

To understand how the process parameters affect melt pool formation, the melt pool area was extracted and analyzed from the thermal videos for all 360 printed tracks. This provided a frame-by-frame view of the melt pool evolution during deposition and enabled consistent comparison of area trends across all parameter combinations.

From the analysis, it was observed that the melt pool area increased significantly with rising laser power. This is most likely because, at higher $P$, more thermal energy was available to melt the powder and substrate, resulting in deeper and longer melt pools. This effect was further amplified when combined with lower scan speeds, which increased the

interaction time between the laser and the material. The combination of high power and low scan speed consistently produced the largest melt pool areas.

When examining scan speed, it was clear that as scan speed increased, the melt pool area decreased. This outcome was expected, as a faster scan speed results in less energy being deposited per unit length, leading to more compact and localized melt pools.

Finally, when analyzing the effect of powder feed rate on melt pool area, the influence was less pronounced but still noticeable. An initial increase in feed rate led to larger melt pools, as more material was available to sustain the melt zone. However, at higher feed rates, the rate of melt pool area growth diminished, and a saturation effect became apparent. This suggests a limit to how much powder can be effectively absorbed by the melt pool.

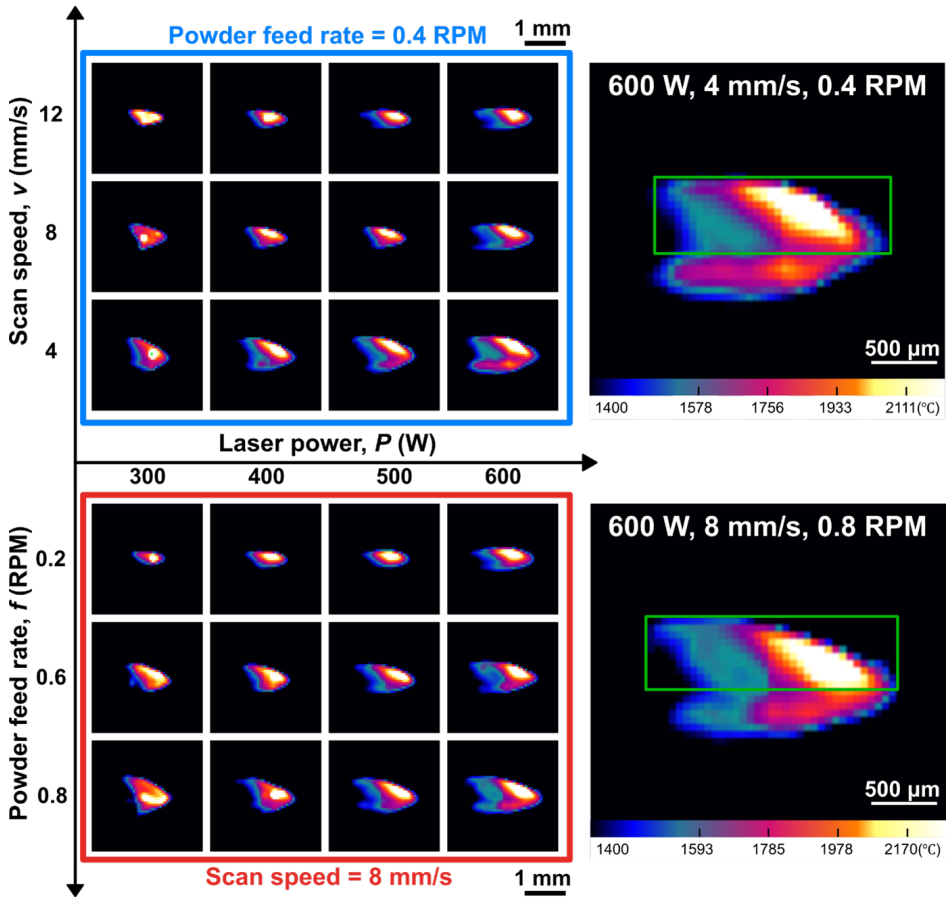


Figure 4: In situ melt pool images captured by the high-speed IR camera across various processing parameters. The top row shows melt pools at a fixed powder feed rate ($f$) of 0.4 RPM with varying laser power ($P$) and scan speed ($v$), while the bottom row shows melt pools at a fixed scan speed ($v$) of 8 mm/s with varying laser power ($P$) and powder feed rate ($f$). The right column presents high-magnification views, highlighting the longitudinal melt pool area (green box), which is the focus of this study.

## 4.2 Melt Track Dimensions

From the post-print 3D surface scans of all melt tracks, a series of static features were extracted to quantify the physical outcome of the deposition process. These included melt track volume, height, and relative surface roughness. All measurements were based on the high-resolution data captured by the automated digital microscope described earlier. While the length of all tracks was fixed at 10 mm, the other dimensions and surface properties varied depending on the processing parameters.

### Melt Track Volume

The analysis showed a strong correlation between melt track volume and both laser power and scan speed. Higher laser power or lower scan speed led to a noticeable increase in melt track volume, likely due to higher linear energy density. Additionally, increasing the feed rate also caused the volume to grow, as more powder was being delivered and melted. This trend was especially evident when using high feed rates in combination with slow scan speeds, which allowed sufficient time for the material to be absorbed into the melt pool.

### Melt Track Height

Similar trends were observed for melt track height, though the relationships were not as strong. In generally, reducing the scan speed or increasing the feed rate consistently led to taller tracks, as more material was being deposited per unit length. However, unexpectedly, melt track height was found to be relatively insensitive to changes in laser power. In some cases, especially those with high power and low scan speed, a slight reduction in track height was observed. This could be attributed to high energy density conditions causing lateral flow in the melt pool. Under such conditions, increased power may enhance surface tension-driven effects such as the Marangoni effect, causing the molten metal to spread outward rather than building vertically.

### Relative Surface Roughness

Relative surface roughness was calculated as the ratio of absolute surface roughness to the mean height of the melt track, to account for variation in size and geometry. A strong correlation was observed between surface roughness and the balance among the three processing parameters.

With increased laser power and scan speed, relative roughness tended to rise. This suggests that high energy input or fast motion may lead to surface irregularities, likely due

to incomplete powder melting, unstable melt pool dynamics, or steep thermal gradients. As for feed rate, increasing it from 0.2 to 0.6 RPM led to smoother surfaces, likely indicating more stable and uniform track formation. However, at 0.8 RPM, surface roughness increased again. This was likely due to excess powder deposition, leading to saturation where the added material could not be fully absorbed, resulting in uneven surface textures.

### Summary

Overall, the melt track dimension analysis confirmed that all three processing parameters, influence geometric features and interact in complex ways that affect melt track morphology.

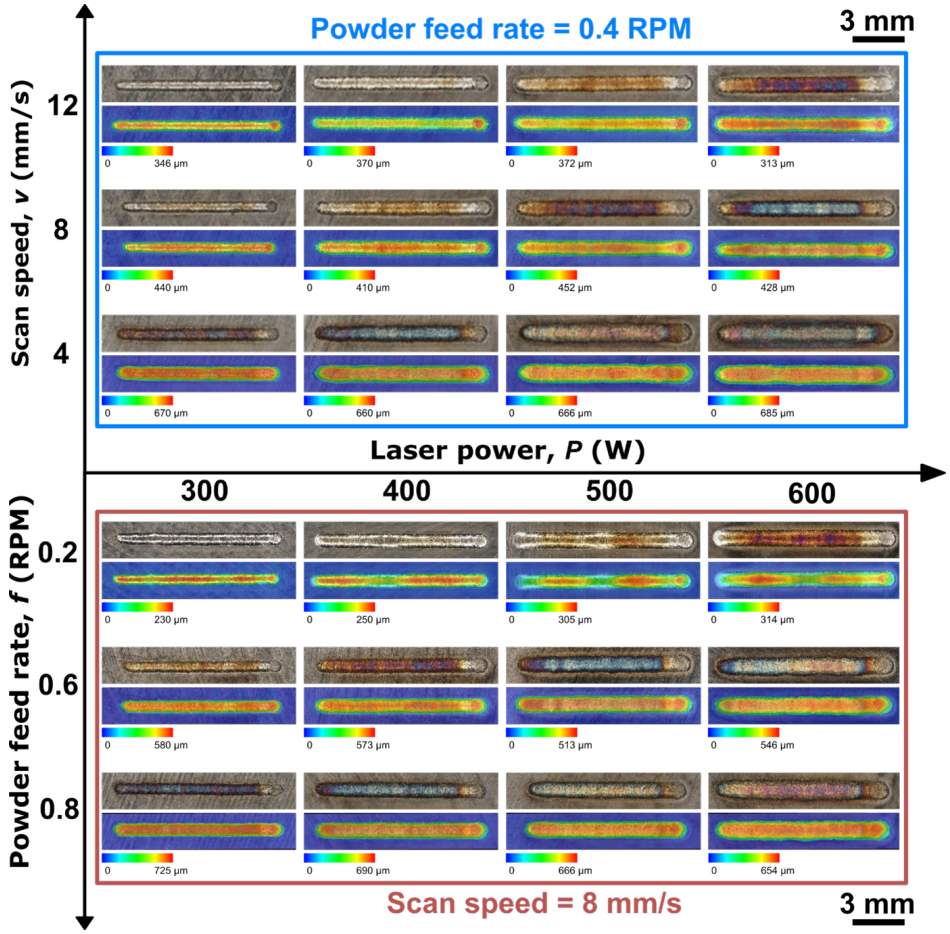


Figure 5: Melt track images and their corresponding 3D geometry under the same processing parameters as in Fig. 4. The 3D geometry provides insights into melt track volume, height, width, and relative surface roughness.

Table 1 summarizes how processing parameters such as laser power ($P$), scan speed ($v$), and feed rate ($f$) influence melt pool and melt track dimensions. It outlines how increasing or decreasing each parameter affects the geometric features observed during the printing

process. For example, the melt pool area increases with higher laser power or feed rate, while it tends to decrease with faster scan speeds. These general trends reflect the overall relationships observed across all experimental trials and provide useful guidance for adjusting parameters to improve print quality in LDED.

Table 1: Influence of increasing laser power ($P$), scan speed ($v$), and powder feed rate ($f$) on melt pool and melt track features, based on experimental observations.

| **Feature** | **Trend** | **Description** |
|---|---|---|
| Melt pool area | $P \uparrow$, $v \downarrow$, $f \uparrow$ | Increases with higher laser power and feed rate; decreases with faster scan speed. |
| Melt track volume | $P \uparrow$, $v \downarrow$, $f \uparrow$ | Strong positive correlation with power and feed rate; slower scan speeds lead to larger volume due to higher energy density. |
| Melt track height | $v \downarrow$, $f \uparrow$ | Generally increases with lower scan speed and higher feed rate; less sensitive to laser power. |
| Relative surface roughness | $P \uparrow$, $v \uparrow$, $f$ unclear | Roughness increases with high power and fast scan speed; no clear trend with feed rate. |

## 4.3 Melt Pool Stability

To capture the dynamic behavior of the printing process, melt pool stability was quantified for all the trials using two key metrics extracted from thermal imaging data: the relative steady-state duration and the coefficient of variation (CV) of the melt pool area. These values were then combined into a single stability score using the equation below:

$$\text{Printing Stability Score} = \frac{\text{CV}}{\text{Relative Steady-State Duration}} \tag{4}$$

Here, the relative steady-state duration (%) refers to the percentage of the total printing time spent in the identified stable region. A longer steady-state duration implies a more sustained and controlled melt pool during the printing process. The CV is defined as the ratio of the standard deviation to the mean melt pool area within this stable region:

$$\text{CV} = \frac{\text{Standard Deviation}}{\text{Mean Melt Pool Area}} \tag{5}$$

A lower CV reflects fewer fluctuations and greater consistency. Therefore, a lower stability score suggests more stable deposition, while a higher score indicates unstable prints with short steady-state periods, significant fluctuations, or both.

From analyzing all parameter combinations, the most stable prints were consistently found at moderate-to-high laser power combined with lower scan speeds. This pattern aligned with trends observed for the melt pool area, where larger and more consistent melt pools were formed under similar conditions. These parameters provided sufficient thermal input and slower traversal, allowing the melt pool to maintain a consistent size and energy throughout the printing process. For these conditions, the relative steady-state duration was often above 70%, and the coefficient of variation remained low, indicating fewer fluctuations during printing.

When examining the scan speed, it was observed that the steady-state duration decreased and fluctuations became more significant as the scan speed increased. Many of the high scan speed prints exhibited noisy signals with short steady-state periods, resulting in high coefficient of variation values and, consequently, higher stability scores.

Finally, for the powder feed rate, no consistent trend was observed, unlike the melt pool area. At low feed rates, the melt pools were smaller but often more consistent and stable, particularly at low-to-mid power levels. As the feed rate increased, some high-power and low scan speed prints maintained stability. However, in other cases, a high feed rate introduced more erratic melt pool behavior, likely due to poor absorption or excessive powder accumulation. This negatively affected the coefficient of variation and reduced the relative steady-state duration.

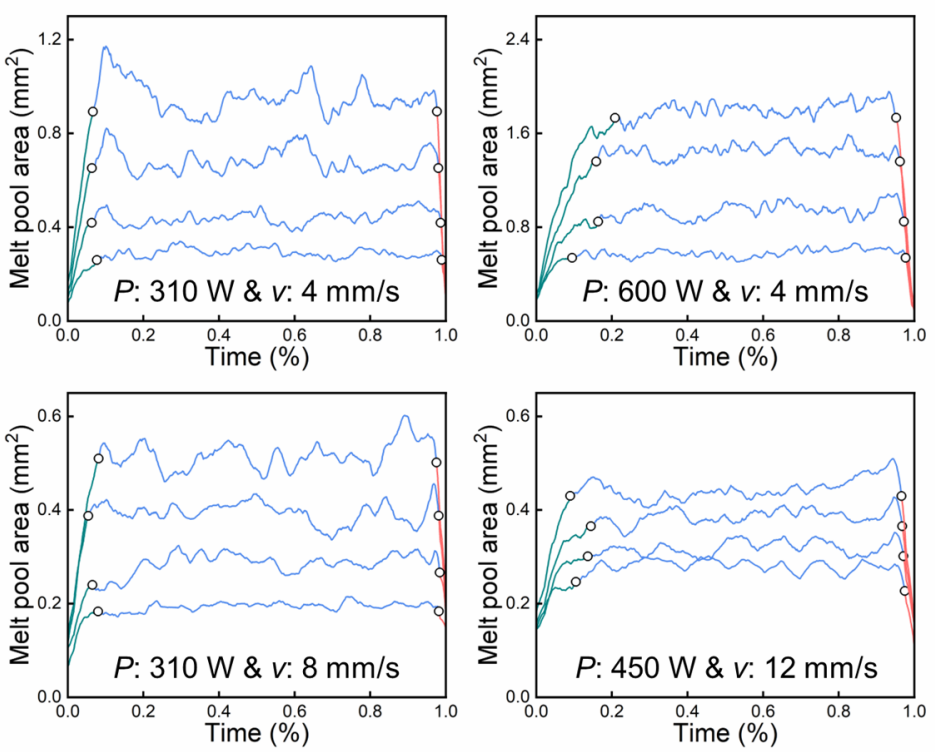


Figure 6: Fluctuations of melt pool area under different processing parameters. In each figure, the line from bottom to top represents the results as the $f$ increases from 0.2 RPM to 0.8 RPM with a fixed $P$ and $v$. Printing stability is quantified by the ratio of the relative duration of the steady-state printing and the coefficient of variations within this region.

Overall, this analysis confirms that melt pool stability is not governed by any single parameter, but rather by the interaction of multiple factors. The combined use of the coefficient of variation and relative steady-state duration provides a robust method to assess stability across varying process conditions.

## 4.4 Melt Pool Morphology and Sputter Density

To explore additional dynamic indicators of print quality, melt pool morphology and sputter density were evaluated across the same dataset. However, no clear correlation was observed between these features and either print quality or process parameters.

### Melt Pool Morphology

For each experiments, the overlap between the actual melt pool shape and the expected elliptical profile was calculated. Theoretically, consistent overlap would indicate a stable and symmetric melt pool. However, analysis showed no observable trend with the processing

parameters. Both high- and low-overlap prints were seen in cases of both good and poor print quality.

This lack of consistency suggests that the melt pool shape is not a reliable indicator of deposition quality. It is possible that the morphological variations arise from local thermal noise or unknown optical distortions, rather than reflecting true instability in the printing process.

#### Sputter Density

Sputter density was defined as the total number of high-temperature pixels detected outside the melt pool region. Similar to melt pool morphology, no consistent or interpretable trend was observed. While some prints with high sputter density corresponded to unstable deposition or high surface roughness, these occurrences were not repeatable across the full range of process parameters. Likewise, prints with low sputter density did not consistently perform better or worse.

These findings suggest that sputter density, like melt pool morphology, is not a dependable indicator of print quality. It may instead be influenced by factors such as local powder distribution or transient disturbances rather than by the processing parameters themselves.

#### Summary

Overall, melt pool morphology and sputter density did not demonstrate reliable relationships with print quality or processing parameters. Although both features were extracted and evaluated across all samples, their lack of consistent trends led to their exclusion from the machine learning models. These results highlight the importance of selecting features that exhibit strong and reproducible correlations with print quality, rather than relying on intuitive or purely visual indicators.

## 4.5 Machine Learning Results

As outlined in the methodology, four feature-based models were trained to predict print quality using different combinations of dynamic and static features: melt track height, melt pool area, melt pool stability, and melt pool stability with surface roughness. Each feature set was evaluated using four regression models, Linear Regression (LR), Decision Tree (DT), Extra Trees (ET), and Neural Network (NN).

Model performance was assessed using three standard metrics: Root Mean Square Error (RMSE), Mean Absolute Percentage Error (MAPE), and the coefficient of determination

($R^2$ score). These metrics were used to quantify the magnitude of prediction error and the explanatory power of each model.

The results for each feature combination are presented below, offering insights into how each type of feature contributes to predictive accuracy across different regression models.

### Model 1 – Melt Track Height

The first model was trained to predict melt track height directly from the input processing parameters. This model focused on a specific static geometric feature and evaluated how effectively it could be predicted.

Table 2: Regression performance for predicting melt track height using different machine learning models.

| Model | RMSE | MAPE |
|---|---|---|
| Linear Regression | 0.057 | 0.17 |
| Decision Tree | 0.027 | 0.05 |
| Extra Trees | 0.024 | 0.055 |
| Neural Network | 0.025 | 0.056 |

The results indicate that both the Extra Trees and Neural Network models achieved the lowest RMSE and MAPE values. This suggests that the relationship between the processing parameters and melt track height is likely non-linear, making it difficult for simpler models such as Linear Regression to capture the underlying dependencies.

The Decision Tree model showed moderate performance but was outperformed by ensemble-based and deep learning approached, highlighting the advantages of model aggregation and deeper learning architectures in modeling complex patterns.

### Model 2 – Melt Pool Area

Similar, to the previous model, this model predicted the melt pool area using the input processing parameters. As a critical indicator of heat input and material interaction, understanding the melt pool area is essential for evaluating print stability and consistency.

Table 3: Model performance for melt pool area prediction using different regression algorithms.

| **Model** | **RMSE** | **MAPE** |
|---|---|---|
| Linear Regression | 0.076 | 0.28 |
| Decision Tree | 0.044 | 0.09 |
| Extra Trees | 0.041 | 0.08 |
| Neural Network | 0.043 | 0.08 |

Once again, both the Extra Trees and Neural Network models outperformed the others, achieving the lowest RMSE and MAPE values. This indicates that the relationship between the input parameters and melt pool area is complex and non-linear. The high error values observed in the Linear Regression model reinforce this point, as it failed to account for the intricate thermal and material interactions involved. Ensemble-based tree models and deep learning approaches, which are better suited to capturing these complexities, demonstrated significantly improved predictive accuracy.

### Model 3 – Melt Pool Stability

The third model focused on predicting the melt pool stability which was calculated from the coefficient of variation and steady-state duration of the melt pool area signal. This metric reflects how consistent the melt pool behavior was during the print.

Table 4: Performance metrics for melt pool stability prediction using process parameters.

| **Model** | **RMSE** | **MAPE** | $\boldsymbol{R^2}$ |
|---|---|---|---|
| Decision Tree | 3.67 | 0.20 | 0.30 |
| Extra Trees | 3.77 | 0.20 | 0.26 |
| Linear Regression | 3.77 | 0.20 | 0.23 |
| Neural Network | 3.82 | 0.21 | 0.24 |

Surprisingly, the Decision Tree model achieved the best overall performance, with the lowest RMSE and highest $R^2$ score of 0.30. This suggests that the relationship between processing parameters and melt pool stability is moderately non-linear, making tree-based models more suitable.

As shown in (Figure 7), the neural network model exhibited a smooth and convergent training loss curve. Permutation feature importance (Figure 8) and corresponding tree-based importance plots (Figures 11 and 15) consistently highlighted scan speed and feed rate as the dominant predictors. Residual plots for Decision Tree (Figure 12), Extra Trees (Figure 16), and Linear Regression (Figure 19) confirmed model errors were randomly distributed for tree-based regressors, while Linear Regression struggled to generalize across the parameter space.

These findings underscore the challenge of capturing dynamic behavior using processing parameters alone, as reflected by the relatively low $R^2$ values across all models. While scan speed and feed rate consistently emerged as primary drivers of melt pool stability, the limited predictive power suggests that additional features may be necessary to fully explain and model stability behavior.

### Model 4 – Melt Pool Stability + Surface Roughness

The final model aimed to evaluate the potential of predicting a combined print quality score derived from both melt pool stability and surface roughness using only the processing parameters. The main goal was to assess whether this fusion of dynamic and static features would provide a more complete and accurate representation of overall print quality.

Table 5: Performance metrics for predicting melt pool stability and surface roughness using process parameters.

| **Model** | **RMSE** | **MAPE** | $\boldsymbol{R^2}$ |
|---|---|---|---|
| Decision Tree | 0.0506 | 0.2181 | 0.8473 |
| Extra Trees | 0.0504 | 0.2130 | 0.8484 |
| Linear Regression | 0.0767 | 0.2605 | 0.6496 |
| Neural Network | 0.0503 | 0.2261 | 0.8493 |

Among all models, this configuration demonstrated the best predictive performance. The Neural Network model outperformed the others, achieving the lowest RMSE and the highest $R^2$ score. Both the Decision Tree and Extra Trees models also performed well, indicating that ensemble methods are effective for capturing the joint behavior of dynamic and geometric factors.

The neural network's training curve (Figure 9) showed smooth convergence with no overfitting, while feature sensitivity (Figure 10) reaffirmed scan speed and feed rate as dominant contributors—mirroring trends observed in the simpler stability-only model.

Consistent patterns were observed across tree-based regressors as well. Feature importance plots from the Extra Trees and Decision Tree models (Figures 17, 13) showed strong dependence on scan speed and feed rate, with minimal contribution from laser power. Residual plots (Figures 18, 14, 20) confirmed that model errors were distributed relatively uniformly for the best-performing regressors, while the linear model exhibited higher variance and underfitting.

These collective results highlight the value of fusing dynamic and static features when predicting overall print quality. The model's high performance, particularly when scan speed and feed rate are emphasized, confirms that these two parameters are critical levers for achieving consistent, high-quality deposition. This also suggests that hybrid metrics, which encode both real-time behavior and surface outcomes, are particularly well-suited for predictive frameworks in LDED.

**Summary**

All four models developed in this study used processing parameters to predict different indicators of print quality. Melt track height was predicted with high accuracy across all regression models, indicating a strong relationship with input settings. Melt pool area predictions showed weaker performance, likely due to higher variability in thermal behavior.

Stability predictions were better captured by non-linear models, though the overall performance suggests that additional features may improve predictions. The best results came from combining melt pool stability with surface roughness, where both tree-based models and neural networks delivered the highest accuracy.

Feature sensitivity plots and feature importance rankings across neural networks and tree-based models revealed consistent trends: scan speed and feed rate were the dominant factors influencing predictions, while laser power consistently had a marginal effect. These patterns held true across both the single-feature (stability) and hybrid (stability + surface roughness) tasks. Training loss curves for neural networks showed stable convergence with no signs of overfitting, and residual plots for tree-based models confirmed that prediction errors were minimal and evenly distributed when non-linear models were used.

Overall, these findings demonstrate that integrating dynamic and static features provides the most accurate and robust approach to predicting print quality using only process parameters.

# 5 Discussion

This study highlights the complex interplay between energy input and material delivery in the Laser Directed Energy Deposition (LDED) process. While the effects of laser power ($P$), scan speed ($v$), and powder feed rate ($f$) are well-documented [4, 9], our findings emphasize that the balance among these inputs, not their individual magnitudes—determines deposition quality. Deviations from optimal energy-material interaction were observed to induce thermal instabilities, manifesting as melt pool fluctuations and inconsistent track geometry. These findings reinforce the notion of LDED as a thermally dynamic and feedback-sensitive system [12, 13].

Among the evaluated features, melt pool stability emerged as a particularly informative dynamic indicator of print quality. In contrast to static metrics such as melt track height or surface roughness, which provide post-process assessments, melt pool stability captured in situ temporal fluctuations that preceded the onset of visible defects. Oscillatory melt pool behavior often anticipated rough or asymmetric track formation, suggesting its value

as an early warning metric. This observation is consistent with prior studies linking thermal instability to subsurface porosity and lack-of-fusion defects [18, 25].

Conversely, not all dynamic features proved equally useful. Morphology and sputter density, despite their distinct visual characteristics, showed poor correlation with print quality across the dataset. These features were likely confounded by noise from uncontrolled sources such as stochastic powder flow, gas turbulence, or surface irregularities. Their low signal-to-noise ratio indicates that, in isolation, they are unreliable predictors of deposition quality, highlighting the need for sensor fusion strategies that combine thermal, optical, and acoustic modalities to robustly infer process state [23, 22].

Machine learning (ML) results provided further evidence for the predictive asymmetry among features. Models trained solely on process parameters could predict static outcomes like melt pool area and track height with moderate accuracy, achieving mean absolute percentage errors (MAPE) below 6% and $R^2$ values above 0.6 in the best cases (Table 2, Table 3). However, their ability to capture dynamic behaviors such as melt pool stability was limited, with the baseline parameter-only model achieving an $R^2$ of just 0.30. This gap underscores the influence of latent variables—such as transient gas flow shifts, powder consistency, or nozzle condition—which are not captured in nominal input parameters.

The most successful model in this study integrated melt pool stability with post-process surface roughness and achieved an $R^2$ of 0.85 using neural networks and ensemble methods (Table 5). This hybrid feature set significantly improved prediction accuracy, suggesting that surface roughness encodes historical thermal fluctuations that directly affect deposition outcomes. This aligns with the idea of "feature memory"—where static metrics can indirectly reflect the history of dynamic process behavior. Such hybrid approaches can be especially powerful for non-destructive quality assurance, where both real-time monitoring and post-process analysis are available.

In addition to strong performance metrics, the residual plots and feature importance diagrams provided further insights into model behavior. For the melt pool stability task, residuals from tree-based models (Appendix 14, 16) appeared centered with relatively uniform spread, suggesting that these models generalized well across the test data. In contrast, the residuals from the linear regression model (Appendix 19) displayed noticeable dispersion patterns and curvature, highlighting its limitations in capturing the non-linear dynamics inherent in melt pool behavior.

Feature importance analyses across both single and hybrid-feature tasks consistently ranked scan speed and feed rate above laser power (Appendix Figures 11 to 17). These findings aligned with neural network permutation sensitivity results (Figures 8, 10), offering cross-model confirmation that deposition quality is more sensitive to material delivery

dynamics than to energy input alone. This reinforces the understanding of LDED as a flow-governed process, where synchronization between powder feed and melt pool evolution plays a critical role in maintaining thermal stability and geometric consistency.

Beyond prediction accuracy, the results also draw attention to the trade-offs between model performance and interpretability. Neural networks outperformed other regressors, but tree-based models like Extra Trees offered clearer insights into feature importance and model behavior. In industrial applications where explainability is critical—such as aerospace or biomedical part production—such transparency may outweigh marginal gains in accuracy. This further supports the use of hybrid models like physics-informed neural networks or interpretable ensemble architectures in future work.

Importantly, this study also demonstrates that high predictive performance requires not just good features, but robust ones. The limited utility of morphology and sputter density, even when modeled using advanced algorithms, emphasizes the need to prioritize features that are both informative and resilient to noise. Investing in higher-resolution, noise-tolerant sensing (e.g., narrow-band IR or structured-light systems) may therefore offer better returns than simply expanding the feature set.

Finally, while the dataset used in this study was limited to single-layer depositions, this constraint was deliberate and justified. Thin-walled geometries, which are prone to failure due to their low thermal mass and minimal structural redundancy, are highly sensitive to layer-level instabilities [4, 5]. As such, the insights gained from these trials are directly applicable to critical use cases in aerospace and biomedical manufacturing. Nonetheless, generalizing to thicker or more complex parts will require future studies incorporating multi-layer trials and diverse material systems. The inclusion of simulated datasets based on physics-driven models [15, 27] may also enable better extrapolation to edge cases not easily observed in controlled experiments.

Taken together, this work reframes the role of machine learning in LDED as more than a predictive tool, it is a mechanism for revealing the hidden dynamics of the process. In doing so, it suggests a new direction for process monitoring: one focused not on static thresholds, but on the consistency of dynamic behavior over time. As the field moves toward real-time adaptive control, the ability to detect instability before defects form will be central to achieving reliable, high-quality additive manufacturing.

# 6 Future Work

While this study established a strong foundation for *in situ* monitoring and data-driven modeling of the LDED process, several opportunities remain for further advancing this research.

One promising direction is to expand the size and diversity of the dataset by incorporating a wider range of parameter combinations, multi-layer builds, and varied geometries. These additions would enhance the robustness and generalizability of the models, helping to better understand how process dynamics evolve over time in more complex build scenarios. This effort could be complemented by exploring additional predictive features beyond melt pool area, stability, and surface roughness. Potential new features may include frequency-domain analysis of thermal signals, advanced morphological or texture descriptors, or temporal trends in geometric features.

Another avenue involves the use of physics-based simulations such as finite element methods or computational fluid dynamics (CFD). These techniques could offer insights into fundamental mechanisms such as thermal gradients, Marangoni flow, and particle interactions. Although simulations are computationally intensive and require accurate calibration, they offer a level of detail that is difficult to achieve through empirical observation alone. As such, they should be viewed as complementary tools to experimental approaches rather than replacements.

The integration of acoustic monitoring is another area worth exploring. Acoustic signals may carry information related to sputtering, porosity formation, or crack propagation—phenomena that may not be easily detected in thermal imaging alone. Combining thermal and acoustic sensing could provide a more holistic understanding of melt pool dynamics and overall print quality.

Extending the framework to different materials would also be valuable. Each material exhibits unique behavior under laser processing due to intrinsic properties such as thermal conductivity, reflectivity, and viscosity. Investigating these effects would contribute to the development of generalized monitoring and control strategies that are material-independent.

Ultimately, the integration of multi-modal sensing, larger and more diverse datasets, and hybrid modeling approaches will bring the field closer to achieving real-time, closed-loop control systems. These systems would be capable of autonomously adjusting processing parameters to ensure consistent, high-quality deposition in LDED applications.

# 7 Conclusion

This thesis developed and evaluated a framework for assessing and predicting print quality in Laser Directed Energy Deposition (LDED) using high-throughput experiments, *in situ* monitoring, and machine learning. By extracting dynamic features such as melt pool stability and static features like melt track height and surface roughness, the study explored how processing parameters—laser power, scan speed, and feed rate—affect deposition behavior.

The results confirmed that achieving stable, high-quality printing depends on maintaining a careful balance between energy input and powder delivery. While traditional geometric metrics like melt pool area and track volume followed expected trends with process conditions, dynamic indicators such as melt pool stability offered deeper insight into real-time process behavior. Secondary features, including melt pool morphology and sputter density, showed limited correlation to print quality and were therefore not used for predictive modeling.

Machine learning models trained on both individual and combined features demonstrated that integrating dynamic and static data significantly improves prediction accuracy. The most successful model combined melt pool stability and surface roughness, emphasizing the importance of leveraging both *in situ* thermal data and post-process measurements for robust quality assessment.

Additionally, the automated data collection and processing workflow developed in this work proved to be both efficient and scalable. It reduced manual effort while enabling systematic exploration of a wide parameter space—an essential capability for real-time implementation.

In summary, this work highlights the potential of data-driven strategies to improve process understanding and control in LDED. It provides a strong foundation for future development of real-time, closed-loop systems and offers a pathway toward optimized thin-wall fabrication with reduced trial-and-error in parameter selection.

# References


[1] M. Rodríguez-Martín, R. Domingo, and J. Ribeiro. Mapping and prospective of additive manufacturing in the context of industry 4.0 and 5.0. *Rapid Prototyping Journal*, 2024.

[2] W.J. Sames et al. The metallurgy and processing science of metal additive manufacturing. *International Materials Reviews*, 61(5):315–360, 2016.

[3] J.J. Lewandowski and M. Seifi. Metal additive manufacturing: a review of mechanical properties. *Annual Review of Materials Research*, 46, 2016.

[4] X. Zhou et al. Forming-based geometric correction methods for thin-walled metallic components: A selective review. *The International Journal of Advanced Manufacturing Technology*, 128(1-2):17–39, 2023.

[5] M.J. Kim and C. Saldana. Thin wall deposition of in625 using directed energy deposition. *Journal of Manufacturing Processes*, 56:1366–1373, 2020.

[6] D. Weisz-Patrault, P. Margerit, and A. Constantinescu. Residual stresses in thin walled-structures manufactured by directed energy deposition: In-situ measurements, fast thermo-mechanical simulation and buckling. *Additive Manufacturing*, 56:102903, 2022.

[7] D. Herzog, V. Seyda, E. Wycisk, and C. Emmelmann. Additive manufacturing of metals. *Acta Materialia*, 117:371–392, 2016.

[8] Hong Zhang, Jianzhong Ma, and Jie Chen. A review of defects in metal additive manufacturing and their detection methods. *Materials*, 13(3):543, 2020.

[9] Chunli Qiu, Chinnapat Panwisawas, Martin Ward, et al. Effect of process parameters on geometrical features and deposition quality during direct energy deposition. *Additive Manufacturing*, 30:100922, 2019.

[10] S. Wang et al. Multi-physics modeling of direct energy deposition process of thin-walled structures: defect analysis. *Computational Mechanics*, 67:1229–1242, 2021.

[11] M.W. Vaughan et al. Development of a process optimization framework for fabricating fully dense advanced high strength steels using laser directed energy deposition. *Additive Manufacturing*, 67:103489, 2023.

[12] J. Haley et al. Review of in situ process monitoring for metal hybrid directed energy deposition. *Journal of Manufacturing Processes*, 109:128–139, 2024.

[13] S.K. Everton, M. Hirsch, P. Stravroulakis, R.K. Leach, and A.T. Clare. Review of in-situ process monitoring and in-situ metrology for metal additive manufacturing. *Materials & Design*, 95:431–445, 2016.

[14] Gustavo Tapia and Alaa Elwany. A review on process monitoring and control in metal-based additive manufacturing. *Journal of Manufacturing Science and Engineering*, 136 (6):060801, 2014.

[15] Y. Huang, M.B. Khamesee, and E. Toyserkani. A new physics-based model for laser directed energy deposition (powder-fed additive manufacturing): From single-track to multi-track and multi-layer. *Optics & Laser Technology*, 109:584–599, 2019.

[16] A. Aggarwal, P.M. Pandey, A.K. Aggarwal, and C.P. Paul. Role of impinging powder particles on melt pool hydrodynamics, thermal behaviour and microstructure in laser-assisted ded process: a particle-scale dem–cfd–ca approach. *International Journal of Heat and Mass Transfer*, 158:119989, 2020.

[17] A. Da Silva, J. Frostevarg, and A.F.H. Kaplan. Thermal monitoring for directed energy deposition of stainless steel, bronze, and cobalt-based alloy. *Surface and Coatings Technology*, 451:129078, 2022.

[18] K. Zhang, Y. Yang, Y. Tian, H. Zhang, B. Zhang, B. Qian, J. Wang, and X. Chen. Pore evolution mechanisms during directed energy deposition additive manufacturing. *Nature Communications*, 15(1):1715, 2024.

[19] S.J. Altenburg, D. Wolff, S. Kleszczynski, D. Werschmoeller, N.S. Tiedje, and K. Willner. In-situ monitoring of a laser metal deposition (lmd) process: Comparison of mwir, swir and high-speed nir thermography. *Quantitative InfraRed Thermography Journal*, 19(2):97–114, 2022.

[20] X. Shang, B. Liu, J. Chen, W. Wu, and B. Zheng. Accurate inverse process optimization framework in laser directed energy deposition. *arXiv preprint arXiv:2407.17338*, 2024.

[21] A. Wang, Y. Liu, C. Zhang, Y. Li, Z. Yu, Y. Liu, X. Zhao, and C. Yang. Blue laser directed energy deposition of aluminum with synchronously enhanced efficiency and quality. *Additive Manufacturing Letters*, 5:100127, 2023.

[22] Anibal Pajares, Hector R Siller, and Alaa Elwany. Multi-sensor framework for online monitoring in directed energy deposition: A review. *Journal of Manufacturing Processes*, 82:725–752, 2022.

[23] Gurkaranbir Sidhu, Hamid Garmestani, and Song Liang. Review of in-process monitoring techniques in direct energy deposition: Current status, challenges, and future directions. *Journal of Manufacturing Processes*, 84:35–57, 2023.

[24] W Gao, Y Zhang, D Ramanujan, et al. The status, challenges, and future of additive manufacturing in engineering. *Computer-Aided Design*, 69:65–89, 2015.

[25] Lei Mi, Yan Zhao, Cheng Chen, Yu Zhang, Song Liang, and Hamid Garmestani. Porosity prediction in directed energy deposition using melt pool thermal features and machine learning. *Additive Manufacturing*, 47:102368, 2021.

[26] Xin Tang, Xiang Yu, Yan Zhao, Yu Zhang, Song Liang, and Hamid Garmestani. Porosity classification using convolutional neural networks on melt pool thermal images in laser directed energy deposition. *Journal of Manufacturing Processes*, 68:1427–1435, 2021.

[27] Q. Wei, H. Wang, X. Chen, J. Yang, Y. Tian, and Y. Li. Transient and steady models for blue laser directed energy deposition. *Journal of Materials Processing Technology*, 325:118292, 2024.

# Appendix A: Model Training and Feature Analysis

## A.1 Neural Network

### A.1.1 Melt Pool Stability

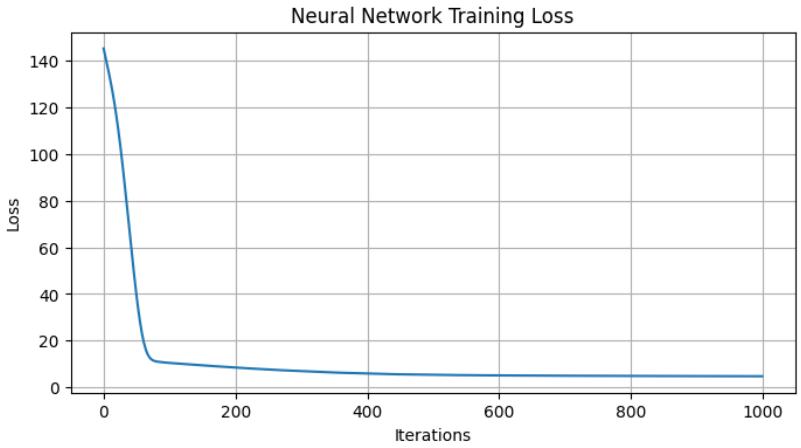


Figure 7: Training loss curve for the neural network model predicting melt pool stability.

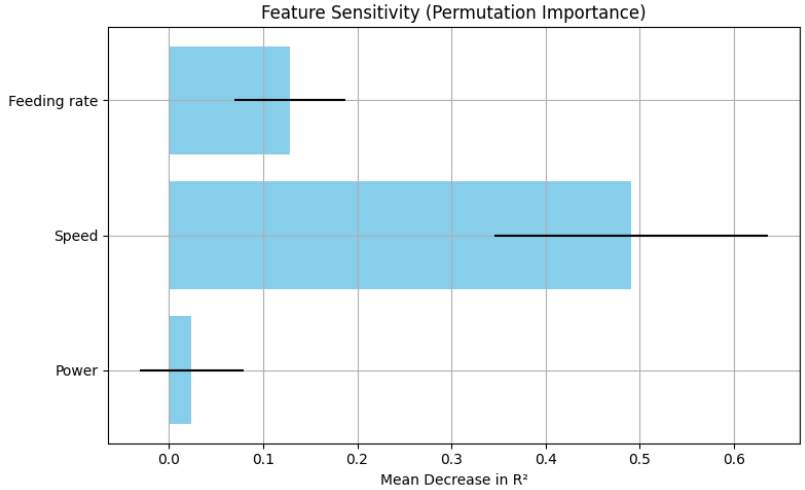


Figure 8: Permutation feature importance for the neural network model (melt pool stability).

### A.1.2 Stability + Surface Roughness

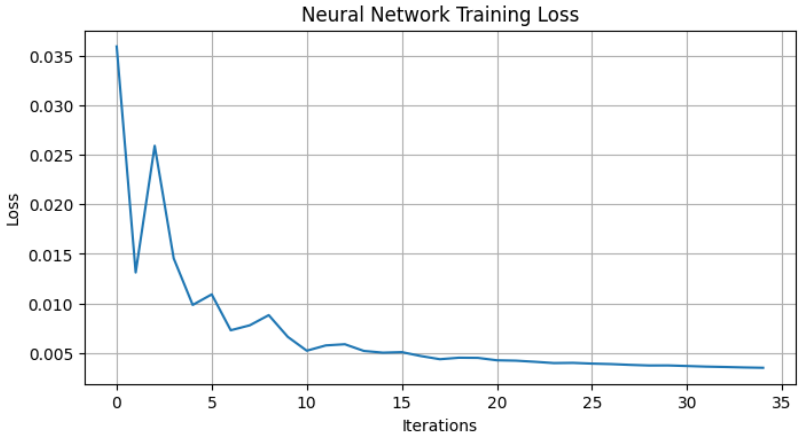


Figure 9: Training loss curve for the hybrid neural network model using melt pool stability and surface roughness.

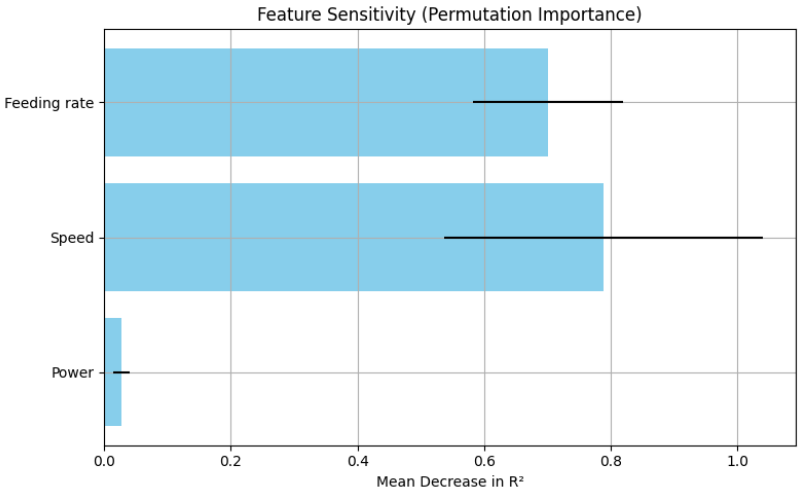


Figure 10: Permutation feature importance for the neural network model (stability + surface roughness).

## A.2 Decision Tree

### A.2.1 Melt Pool Stability

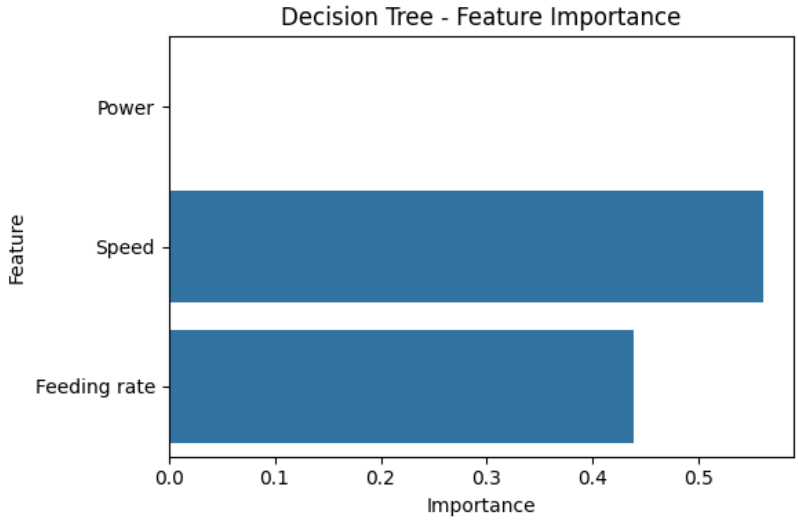


Figure 11: Feature importance for the Decision Tree model (melt pool stability).

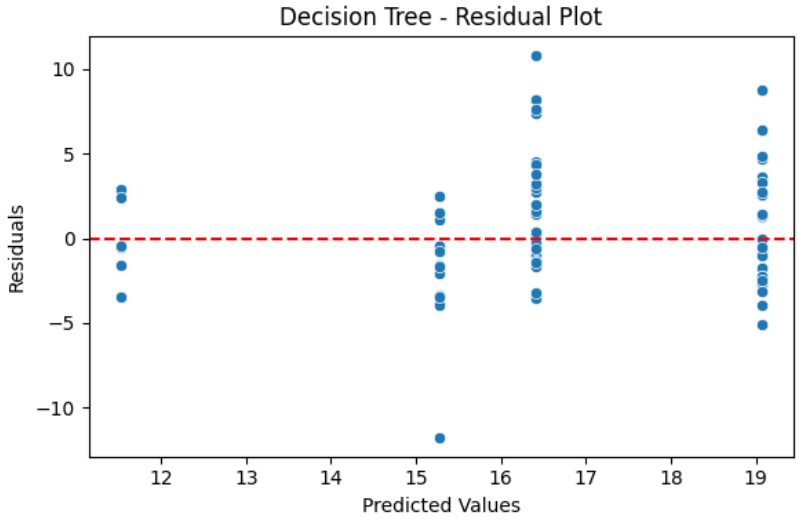


Figure 12: Residual plot for the Decision Tree model (melt pool stability).

### A.2.2 Stability + Surface Roughness

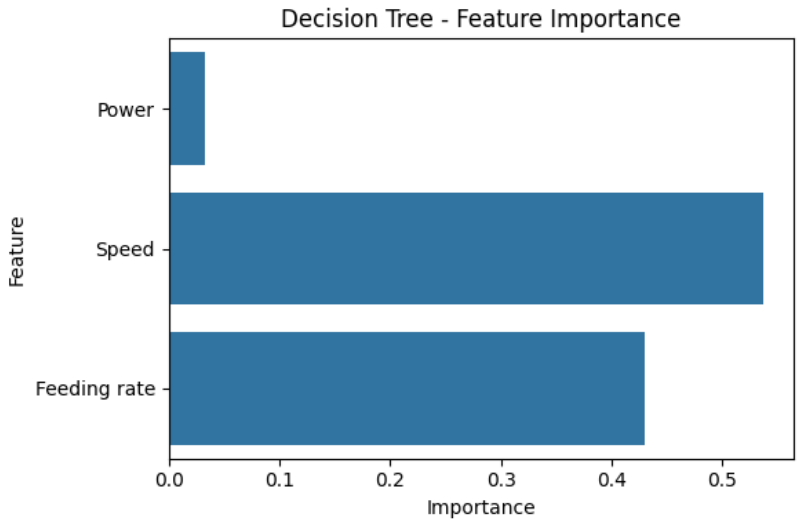


Figure 13: Feature importance for the Decision Tree model (stability + surface roughness).

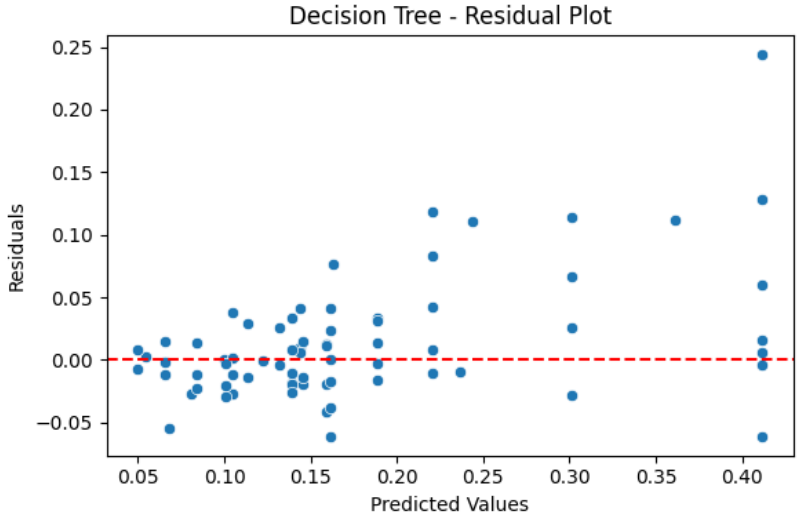


Figure 14: Residual plot for the Decision Tree model (stability + surface roughness).

## A.3 Extra Trees

### A.3.1 Melt Pool Stability

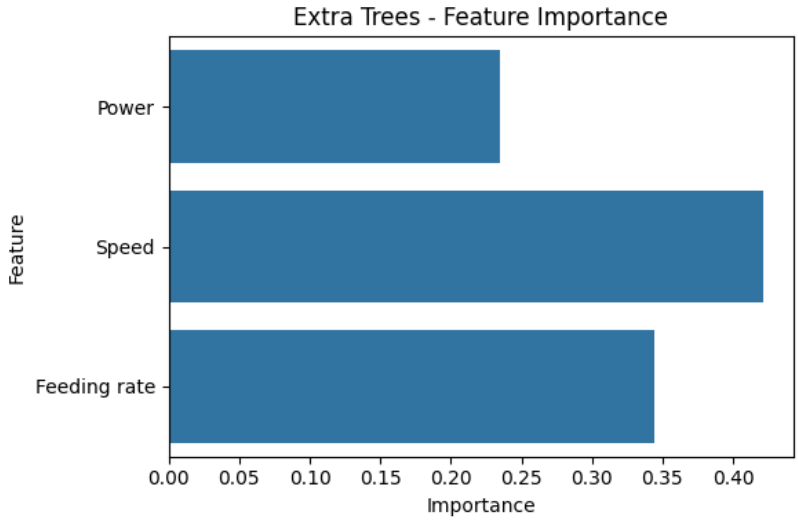


Figure 15: Feature importance for the Extra Trees model (melt pool stability).

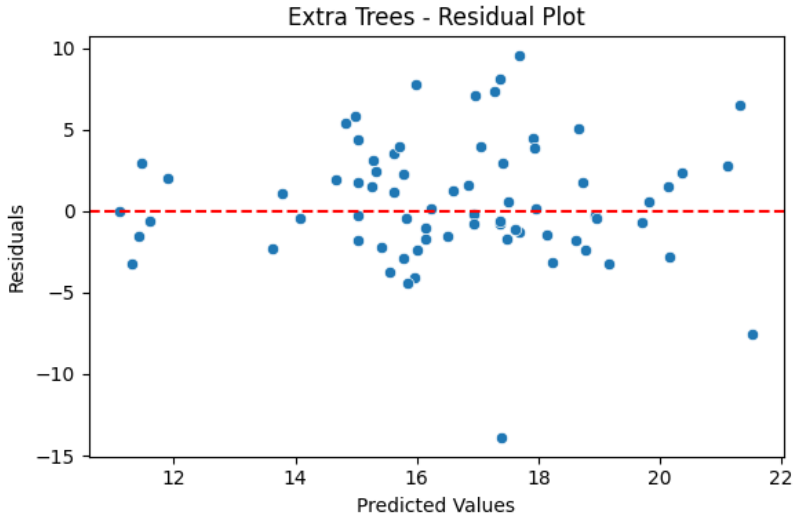


Figure 16: Residual plot for the Extra Trees model (melt pool stability).

### A.3.2 Stability + Surface Roughness

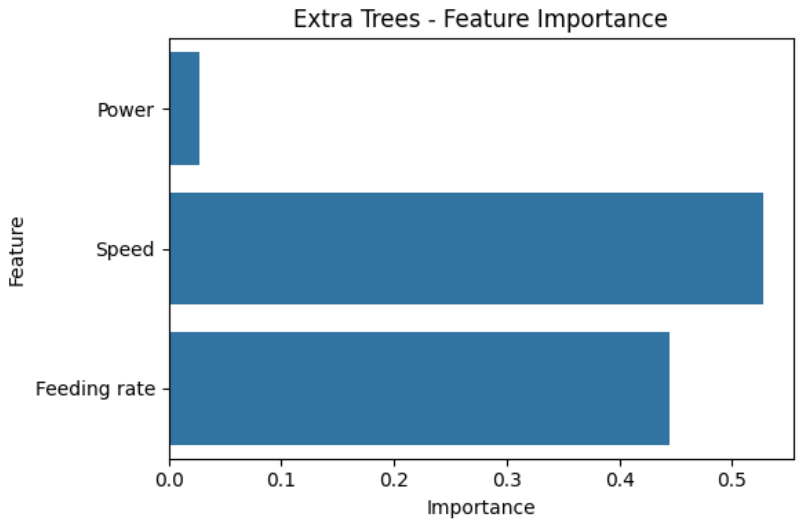


Figure 17: Feature importance for the Extra Trees model (stability + surface roughness).

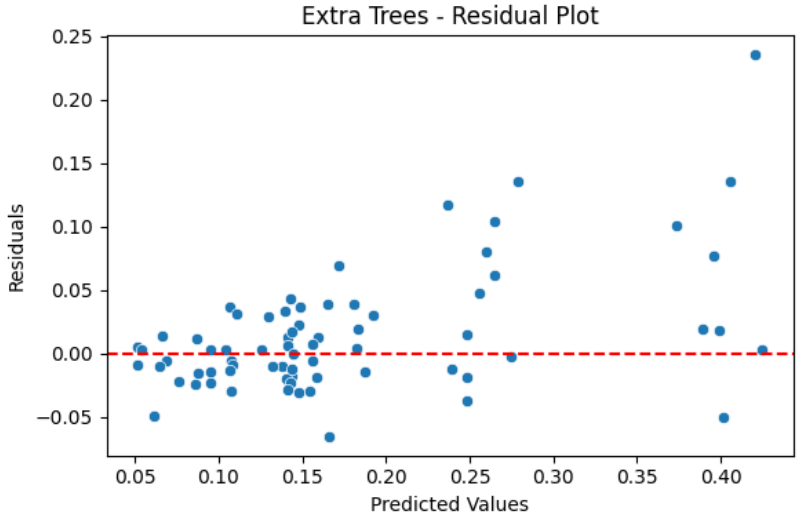


Figure 18: Residual plot for the Extra Trees model (stability + surface roughness).

## A.4 Linear Regression

### A.4.1 Melt Pool Stability

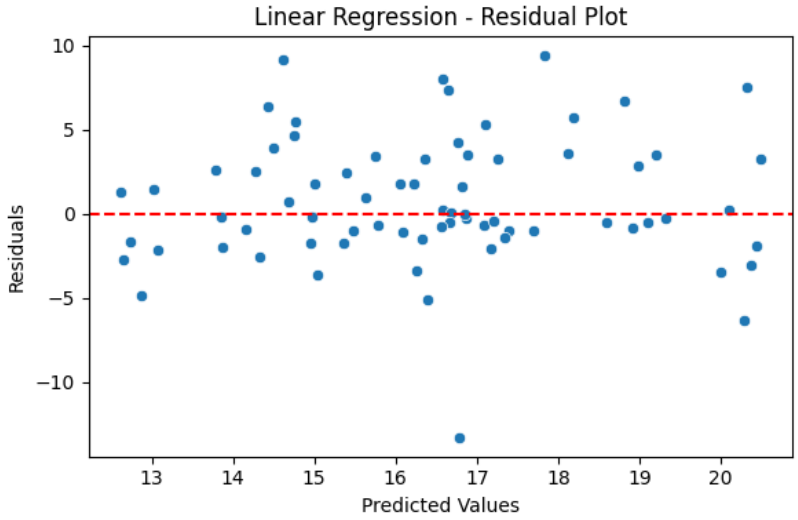


Figure 19: Residual plot for the Linear Regression model (melt pool stability).

### A.4.2 Stability + Surface Roughness

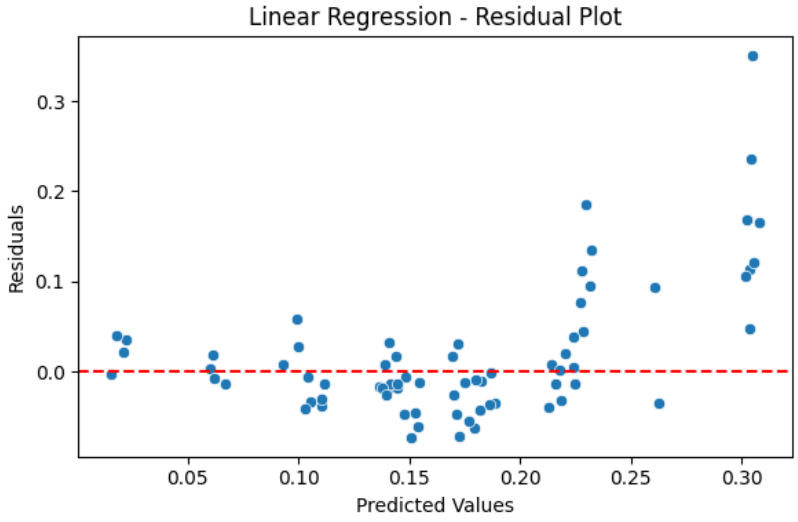


Figure 20: Residual plot for the Linear Regression model (stability + surface roughness).